Identification of two sources of carbon monoxide in comet Hale–Bopp

Michael A. DiSanti*†, Michael J. Mumma†, Neil Dello Russo*†, Karen Magee-Sauer‡, Robert Novak§ & Terrence W. Rettig‖

** Department of Physics, The Catholic University of America, Washington DC 20064, USA*
† Laboratory for Extraterrestrial Physics, NASA Goddard Space Flight Center, Code 690, Greenbelt, Maryland 20771, USA
‡ Department of Chemistry and Physics, Rowan University, Glassboro, New Jersey 08028, USA
§ Department of Physics, Iona College, New Rochelle, New York 10801, USA
‖ Department of Physics and Astronomy, University of Notre Dame, Notre Dame, Indiana 46556, USA

The composition of ices in comets may reflect that of the molecular cloud in which the Sun formed, or it may show evidence of chemical processing in the pre-planetary accretion disk around the proto-Sun. As carbon monoxide (CO) is ubiquitous in molecular clouds[1,2], its abundance with respect to water could help to determine the degree to which pre-cometary material was processed, although variations in CO abundance may also be influenced by the distance from the Sun at which comets formed[3–5]. Observations have not hitherto provided an unambiguous measure of CO in the cometary ice (native CO). Evidence for an extended source of CO associated with comet Halley was provided by the Giotto spacecraft[6–9], but alternative interpretations exist[10]. Here we report observations of comet Hale–Bopp which show that about half of the CO in the comet comes directly from ice stored in the nucleus. The abundance of this CO with respect to water (12 per cent) is smaller than in quiescent regions of molecular clouds, but is consistent with that measured in proto-stellar envelopes[11], suggesting that the ices underwent some processing before their inclusion into Hale–Bopp. The remaining CO arises in the coma, probably through thermal destruction of more complex molecules.

The appearance of comet Hale–Bopp enabled studies of the evolution of cometary activity in unprecedented detail. At large heliocentric distances ($R_h \approx 4$–7 AU), volatile release was driven by CO sublimation[12–14]. However, gas production rates obtained at large R_h do not provide information on the amount of native CO relative to H_2O, the dominant native ice, due to the substantially different volatilities of these two compounds. Closer to the Sun, water sublimation controls the release of all species, and reliable mixing ratios for native ices can be obtained. Our study of water, CO and dust reveals the onset and persistence of a distributed source for CO within 2 AU heliocentric distance, and establishes the relative abundances of water and CO ices in the cometary nucleus.

We observed Hale–Bopp using the cryogenic echelle grating spectrometer (CSHELL)[15] on the NASA IRTF 3-m telescope at Mauna Kea Observatory, Hawaii (Table 1). Cometary line and continuum intensities were obtained from two-dimensional frames (256 spectral pixels (columns) by ~150 spatial pixels (rows)) representing the net (sky-subtracted) comet signal (Fig. 1). Absolute flux calibration was achieved through comparison with the spectra of flux-standard stars. Details of our observing strategy and data processing are given elsewhere[16,17]. The intensity of CO line emission at each point along the slit is proportional to the column density of molecules in the upper state of the transition giving rise to the line. The CO rotational temperature (T_{rot}) was obtained at each position from multiple lines in the $\nu = 1$–0 band (where ν is the vibrational quantum number), using the standard analysis for linear molecules[18] (Table 1).

A one-dimensional distribution of CO molecules about the nucleus was obtained by combining spatial profiles for several CO lines; dust profiles were obtained from simultaneously measured thermal continuum emission (Fig. 2). The spatial distributions of CO and dust were similar when the comet was beyond ~2 AU from the Sun, but the CO emission consistently displayed a more extended profile within ~1.5 AU of the Sun. (An extended CO distribution has also been reported from independent CSHELL observations obtained on UT 1997 March 05 ($R_h = 1.03$ AU pre-perihelion).[19]) If CO and dust were released only from the nucleus, they should have similar spatial profiles over this region of the coma. The much broader extent for CO that first appears at $R_h \approx 1.5$ AU suggests the onset of a second (distributed) source.

Evidence of both native and distributed CO contributions can be seen by examining the effective production rate (Q, molecules s^{-1}) as a function of projected distance from the nucleus (Fig. 3). Production rate curves ('Q-curves') are generated by stepping a 1×1 arcsec aperture along the CO profile, extracting a production

Table 1 CO production in comet Hale–Bopp

UT date	R_h* (AU)	Δ* (AU)	T_{rot}† (K)	Q_{CO}‡ (10^{29} molecules s^{-1})	native/total§	Q_{H_2O}‖ (10^{30} molecules s^{-1})	Q_{CO}/Q_{H_2O}¶	Q_{nat}/Q_{H_2O}#
1996								
13 Jun.	4.11	3.18	20	0.96 ± 0.15				
19 Sep.	3.03	2.92	30	1.28 ± 0.26				
11 Dec.	2.02	2.83	55 ± 9	2.98 ± 0.32				
1997								
21 Jan.	1.48	2.18	94 ± 5	10.78 ± 0.30	0.49	4.00 ± 0.39	0.270 ± 0.027	0.132 ± 0.013
24 Feb.	1.11	1.57	114 ± 6	18.16 ± 0.75	0.48	8.89 ± 0.89	0.204 ± 0.022	0.098 ± 0.011
02 Mar.	1.06	1.47	111 ± 3	19.80 ± 0.57	0.48	7.63 ± 0.23	0.260 ± 0.011	0.125 ± 0.005
10 Apr.	0.93	1.44	105 ± 4	22.31 ± 1.35	0.53	9.99 ± 0.38	0.223 ± 0.016	0.118 ± 0.008
16 Apr.	0.95	1.53	116 ± 4	24.69 ± 2.04	0.46	9.12 ± 0.36	0.271 ± 0.025	0.125 ± 0.011
30 Apr.	1.05	1.75	106 ± 3	14.27 ± 1.00	0.67	6.76 ± 0.33	0.211 ± 0.018	0.141 ± 0.012
01 May.	1.06	1.77	97 ± 3	17.93 ± 0.87	0.53	7.43 ± 0.41	0.241 ± 0.018	0.128 ± 0.009
08 Aug.	2.24	2.90	54 ± 12	2.95 ± 0.37				
25 Sep.	3.08	2.86	30	1.52 ± 0.35				

* Heliocentric and geocentric distances.
† Derived CO rotational temperatures, with uncertainties representing 1σ confidence levels. The rotational temperature increases when moving away from the nucleus, and this is probably the signature of photolytic heating in the intermediate coma, caused primarily by (fast) hydrogen atoms, and/or possibly by electron collisions[25]. Rotational temperatures were determined from line intensities over a range of projected distances from the nucleus corresponding to the 'terminal' portion of the CO Q-curve. For the three dates with $R_h > 3$ AU, T_{rot} was adopted from ref. 26, and an uncertainty of ±5 K has been included in calculating Q_{CO} for these dates.
‡ Total (native + distributed) CO production rate. For each date, Q was calculated line-by-line using g-factors appropriate to the derived rotational temperature. Q_{CO} represents the average for all lines observed, and listed uncertainties represent 1σ stochastic errors and include line-to-line variations. These incorporate 14–20 points per line, and multiple lines per date (compare Fig. 3). As we rely on terminal Q-curve values, this method is independent of possible effects in the inner coma (for example, CO optical depth). Further refinements require modelling the distributed CO source (see text).
§ Amount of total CO as ice native to the nucleus (based on values from the 'native CO' heliocentric fit extrapolated to smaller R_h; compare Fig. 4), divided by Q_{CO}.
‖ Derived water production rate[17], with 1σ errors determined as above (footnote †).
¶ Total Q_{CO} relative to Q_{H_2O}. The mean value for these dates was 0.241 ± 0.009.
# Inferred 'native CO' relative to H_2O. The mean value for these dates was 0.124 ± 0.004. Thus the mean fractional abundance of 'native CO' to total CO was 51 ± 3%.

© 1999 Macmillan Magazines Ltd

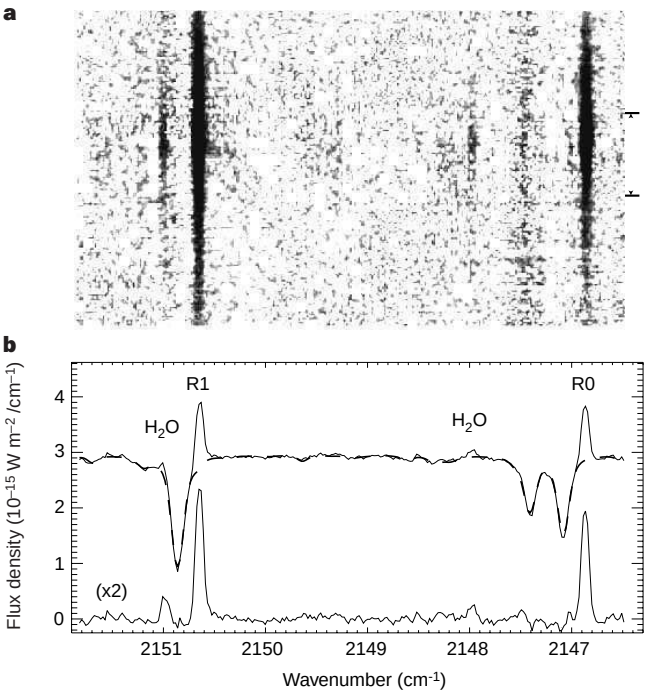

Figure 1 CSHELL spectrum of comet Hale–Bopp, obtained UT 1997 May 01.1. **a**, Sky-subtracted spectral-spatial image. To reveal better the distribution of CO emission along slit, the (extremely bright) dust continuum emission has been removed. The small pixel size (0.2 arcsec) afforded by CSHELL provided seeing-limited (frequently 1 arcsec or better) spatial resolution along the 30-arcsec-long slit, which we oriented east–west. The greater spatial extent of the CO lines, compared with that of the adjacent H_2O emissions (marked in **b**), is evident. The vertical scale to the right of the figure indicates 10^4 km at the comet, and east is at the top. **b**, Top trace: spectral extract (before continuum subtraction) summed over 5 rows (1 arcsec) centred on the peak continuum intensity. Subtraction of the optimized atmospheric model (dashed curve), generated using the Spectrum Synthesis program[27] which accesses the HITRAN-1992 molecular data base[28], yields the observed net cometary molecular emission in excess of the continuum (bottom trace; scaled by 2×). We used a 1-arcsec slit width, resulting in a spectral resolving power $\nu/\Delta\nu \approx 2 \times 10^4$, where ν is the photon wavenumber (cm^{-1}). This was sufficient to isolate line emission in the CO $v = 1$–0 band (near 4.7 μm) from adjacent CO absorption features in the terrestrial atmosphere, and from underlying cometary continuum emission. The telescope was periodically moved 2 arcmin north or south of the comet to sample background sky emission; no cometary CO emission was present in the 'sky' beam at the noise level of the data, based on test observations.

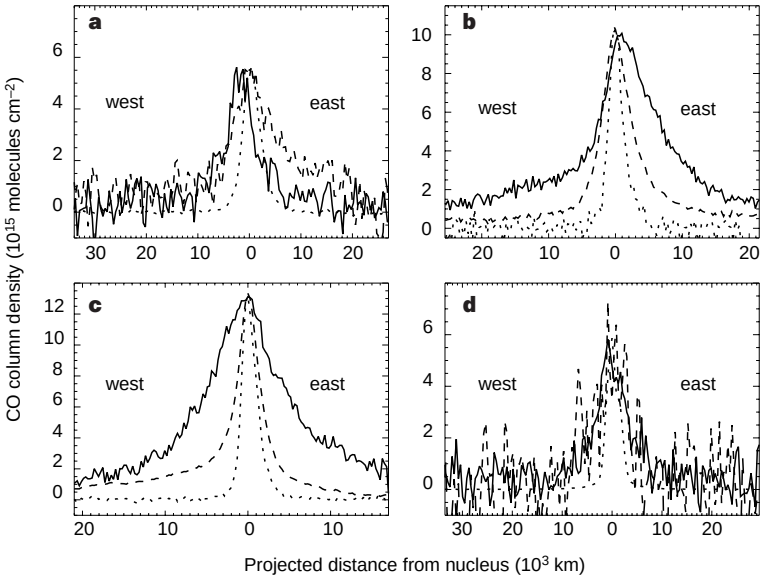

Figure 2 Spatial profiles of CO emission in comet Hale–Bopp. Shown in each panel is the sum of line profiles sampling a range in rotational levels, thereby providing a measure of the overall CO distribution along the slit. **a**, 1996 December 11 ($R_h = 2.02$ AU pre-perihelion); **b**, 1997 January 21 ($R_h = 1.48$ AU pre-perihelion); **c**, 1997 May 01 ($R_h = 1.06$ AU post-perihelion); **d**, 1997 August 08 ($R_h = 2.24$ AU post-perihelion). Scaled continuum (dashed trace) and stellar ('point spread function', dotted trace) profiles are shown for comparison. Note the change in appearance between December and January CO profiles, which we take to signal the onset of the distributed source between 2.0 and 1.5 AU pre-perihelion. At $R_h = 2.02$ AU pre-perihelion, the spatial profile of CO is east–west symmetric, but the dust is more extended towards the east (**a**). At 1.48 AU and 1.06 AU, the CO profile is markedly more extended than the dust in both east and west directions (**b**, **c**). At 2.24 AU post-perihelion, both CO and dust are east–west symmetric and their profiles have the same extent and shape (**d**). The east–west slit orientation was chosen to facilitate peaking up the comet signal in the slit, and for more easily assessing fine adjustments to telescope tracking rates as needed. The spatial profiles of gas and dust are typically averaged over 2–3 h.

© 1999 Macmillan Magazines Ltd

rate at each position, and then averaging values east and west of the nucleus[16]. We take the terminal value of the Q-curve to represent the total production rate Q_{CO} (see Table 1). Analogous curves are generated for dust by stepping along the corresponding continuum profile.

Our model assumes constant outflow velocity, so acceleration in the intermediate coma[20] could influence the shape of our Q-curves. However, the Q-curves for species released at the nucleus should be similarly affected. Those for water and dust are nearly identical in shape, but differ greatly from that of CO inside 2 AU heliocentric distance (Fig. 3b). Although acceleration introduces small increases to our retrieved gas production rates, another cause must be sought for the strong difference between the Q-curves of water and CO. Giotto measured ~25% increase in gas outflow velocity between $\sim 4 \times 10^3$ km and 2×10^4 km from the nucleus of comet Halley[20]. A similar effect in Hale–Bopp would lead to enhanced estimates in Q_{CO} (and Q_{H_2O}) of only 3–4% at 1.48 AU, and 6–8% near perihelion, far smaller than the ~100% increase in Q_{CO} over Q_{H_2O} seen in Fig. 3b. The presence of a distributed source for CO, similar to that inferred for comet Halley[6], is suggested.

The evolution from a purely native source for CO to a combination of native and distributed sources occurs between 2.02 and 1.48 AU pre-perihelion; this is clearly seen by comparing Q-curves for these dates. When release is solely from the nucleus, the Q-curve reaches its terminal value quickly—in this case the curves for dust and CO have similar shapes (Fig. 3a). But when both native and distributed sources are present, as for CO, the Q-curve reaches its terminal value farther from the nucleus (Fig. 3b). The ratio of contributions from native and distributed sources may be estimated by comparing the terminal value of the Q-curve for CO with that for dust and H_2O, these latter Q-curves being proxies for the native source alone.

The dependence of total CO production rate on heliocentric distance (Fig. 4) can also be used to distinguish native from distributed sources. Our observations at $R_h > 2$ AU are consistent with $Q_{CO,nat} = (1.05 \times 10^{30}) R_h^{-1.73 \pm 0.26}$ molecules s^{-1}, which we take to represent the (purely) native contribution to total CO based on the similar spatial extent for CO and continuum profiles. This heliocentric dependence is consistent with that derived for H_2O using the same instrument and approach; our Q-curves for water support its release primarily as a parent volatile from the nucleus[17].

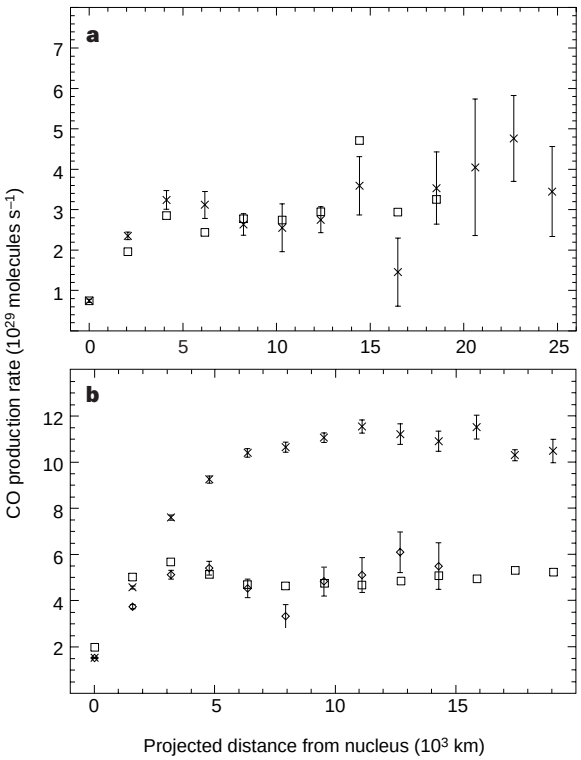

Figure 3 Hale–Bopp production rate curves (Q-curves), showing the derived Q (molecules s^{-1}) as a function of projected distance from the nucleus. The production rate $Q = (Flg)(4\pi\Delta^2/hc\nu\tau)[1/f(x)]$, where F is the emitted line flux (W m^{-2}), g is the fluorescence efficiency (photon s^{-1} molecule^{-1}) at $R_h = 1$ AU (Q depends on T_{rot} through g; ref. 29), Δ is the geocentric distance (m), $hc\nu$ is the energy (J) of a photon with wavenumber ν (cm^{-1}), and τ (s) is the photodissociation lifetime at 1 AU. Under quiet Sun conditions, $\tau_{CO} \approx 1.2 \times 10^6$ s (ref. 30). The quantity $f(x)$ represents the fraction of molecules included in the sampled region, given square pixels (compare ref. 16). We adopt a model in which production occurs only at the nucleus, and assume a uniform outflow velocity (v) of $1{,}100 R_h^{-0.5}$ m s^{-1} (compare refs 13, 26). ($Q \propto v$ as $f(x) \propto 1/v$; see text for the estimated effect of gas acceleration on Q.) The average of Q east and west of the nucleus is shown (crosses, with 1σ uncertainties, denote CO), using a 1×1 arcsec stepped aperture. The corresponding continuum Qs (open squares) are shown for comparison. **a**, 1996 December 11 ($R_h = 2.02$ AU pre-perihelion); **b**, 1997 January 21 ($R_h = 1.48$ AU pre-perihelion). For December, Q_{CO} is based on four lines, and Q was averaged 2–11 arcsec either side of the nucleus; a purely native source is indicated (compare Fig. 2a). For January, ten lines were measured and Q was averaged 4–11 arcsec from the nucleus. Terminal values of scaled continuum (or H_2O, open diamonds) and CO Q-curves are in the ratio 0.49 (compare Table 1 footnote §, and Fig. 4). Figure 3 suggests a significant contribution from the distributed CO component in January which was not present in December.

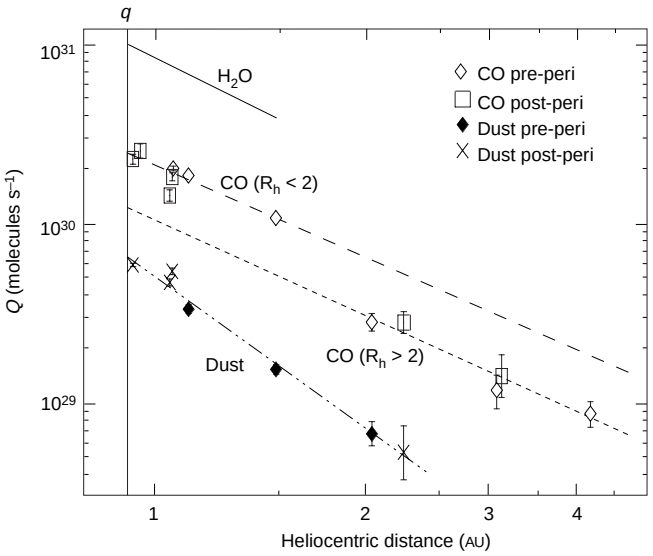

Figure 4 Heliocentric dependence of Q_{CO} and Q_{H_2O} in comet Hale–Bopp. The pre-perihelion increase in CO production between 2.0 and 1.5 AU is evident. A least squares linear fit for $R_h > 2$ AU represents the contribution from native CO (short-dashed line) and has a power-law slope of -1.73 ± 0.26. A fit for $R_h < 2$ AU (long-dashed line) reveals a similar slope (-1.66 ± 0.22), but is displaced upwards by a factor of ~2. These fits imply values of $(1.05 \pm 0.44) \times 10^{30}$ and $(2.07 \pm 0.20) \times 10^{30}$ molecules s^{-1}, respectively, at $R_h = 1$ AU. A fit to Q_{H_2O} (solid line) obeys a power law with slope -1.88 ± 0.18 (ref. 17). Relative dust production (Q_{dust}) was obtained from continuum flux density F_ν (W m^{-2} cm^{-1}) after distinguishing contributions from grain thermal emission [F_ν(th)] and scattered sunlight, using observations obtained near 2.0, 3.35 and 4.7 μm. Q_{dust} was calculated as $F_\nu(\text{th})/B_\nu(T_{dust})$, averaged over CO settings. The Planck function $B_\nu(T) \propto \nu^3/[\exp(x\nu/T) - 1]$, where $x \equiv hc/k \approx 1.44$ cm K, and $T \equiv T_{dust} = 329 R_h^{-0.53}$ (ref. 31). $B_\nu(T_{dust})$ was normalized to unity for $\nu = 2{,}150$ cm^{-1} (4.651 μm) and $R_h = 1$ AU. Q_{dust} obeys a steeper power law than CO, H_2O, or mm-sized dust[32] (-2.73 ± 0.12, assuming that dust and gas outflow velocities vary similarly with R_h) and exhibits no such discontinuity between 2.0 and 1.5 AU as seen for Q_{CO}. This figure suggests that sublimation of native CO and release of the 'parent' species for distributed CO are controlled by sublimation of the same nuclear ice, and that the onset of distributed CO is not explained in terms of increased dust production or dust fragmentation alone. The vertical solid line (indicated by q) marks the perihelion distance (0.914 AU).

© 1999 Macmillan Magazines Ltd

A separate fit for $R_h < 2$ AU ($Q_{CO} = (2.07 \times 10^{30})R_h^{-1.66\pm0.22}$) shows the same heliocentric dependence, and is displaced above the 'native' fit by a factor of ~2. Thus the present analysis suggests approximately equal contributions from native and distributed sources to the total CO production in comet Hale–Bopp within $R_h \sim 1.5$ AU (Table 1).

Could the onset of a distributed source for CO be related to a change in dust production or destruction? Our measurements of dust (at 4.7 μm wavelength) sample particles with sizes of a few micrometres, and follow a heliocentric dependence ($Q_{dust} \propto R_h^{-2.73\pm0.12}$) which is steeper than our findings for Q_{CO} and Q_{H_2O} (see note added in proof, below). This implies a rapid increase in dust fragmentation, and hence a decrease in mean particle size, with decreasing heliocentric distance. (In our analysis, we have assumed the same heliocentric dependence of outflow velocity ($R_h^{-0.5}$) for dust and gas.) Detailed modelling of dust properties (outflow, composition, destruction) convolved with geometrical effects, will be reported elsewhere.

If the onset of distributed CO emission was related to increased dust release as the comet approached perihelion, a sharp increase (that is, a 'jump') in Q_{dust} similar to that observed for Q_{CO} between 2.02 and 1.48 AU would be expected. Whereas Q_{CO} follows two distinct distributions—one for $R_h < 2$ AU and another for $R_h > 2$ AU—Q_{dust} appears to fit a single distribution, with no such jump near (or inside) $R_h = 2$ AU.

The lack of a jump in Q_{dust} near $R_h = 2.0$–1.5 AU demonstrates that the onset of distributed CO emission cannot be explained by increased dust production alone. Rather, it is plausible that a threshold (most likely thermal) is reached for release of additional CO in the coma. The similar power-law dependence exhibited by Q_{CO} for both $R_h < 2$ AU and $R_h > 2$ AU, and by Q_{H_2O} (ref. 17), suggests that release of the 'parent' giving rise to distributed CO is controlled by sublimation of the same nuclear ice as seen for other native volatiles (water, native CO). We thus infer that the distributed parent has a constant mixing ratio in the nucleus relative to native H_2O and CO ices.

The difference between the Q-curves for CO and (scaled) dust approximates the Q-curve for the distributed component alone. This reaches its terminal value at a projected distance $\rho \approx 6.5 \times 10^3$ km from the nucleus for $R_h = 1.48$ AU, and at $\sim 5.1 \times 10^3$ km for $R_h = 1.06$ AU. The distance ρ approximates the scale for release of distributed CO, and can be compared with model predictions to better constrain the scale length of the distributed parent. Future refinements[21–24] to our analytical approach include accounting for axisymmetric outflow and for gas acceleration in the coma. We expect such modelling to have relatively little effect on our retrieved amount of native CO, but it should provide significant improvements to our understanding of the distributed source.

We have characterized the release of carbon monoxide in comet Hale–Bopp, and compared it with water and dust. Within $R_h \approx 1.5$ AU, our results support a dual-source nature for CO production, as seen first in comet Halley during the Giotto spacecraft encounter[6]. We infer a total (native plus distributed) mean CO production rate of 24.1 ± 0.9% relative to water, with 51 ± 3% of the observed CO contained in the nuclear ice, the remainder being produced in the coma.

Note added in proof: Production of millimetre-sized dust in comet Hale–Bopp follows a single distribution with power law $R_h^{-1.7\pm0.2}$ for R_h between 0.9 and 2.5 AU (ref. 32). This heliocentric slope is consistent with those we derive for Q_{CO} and Q_{H_2O}, and this supports uniform mixing of volatile and refractory components in the nucleus. □

Received 17 November 1998; accepted 12 April 1999.

1. Rank, D. M., Townes, C. H. & Welch, W. J. Interstellar molecules and dense clouds. *Science* **174,** 1083–1101 (1971).
2. Turner, B. E. Recent progress in astrochemistry. *Space Sci. Rev.* **51,** 235–337 (1989).
3. Mumma, M. J. Organic volatiles in comets: Their relation to interstellar ices and solar nebula material. *Astron. Soc. Pacif. Conf. Ser.* **122,** 369–396 (1997).
4. Mumma, M. J., Weissman, P. R. & Stern, S. A. in *Protostars and Planets, III* (eds Levy, E. H. & Lunine, J. I.) 1177–1252 (Univ. Arizona Press, Tucson, 1993).
5. Sandford, S. A. & Allamandola, L. J. The condensation and vaporization behavior of H_2O:CO ices and implications for interstellar grains and cometary activity. *Icarus* **76,** 201–224 (1988).
6. Eberhardt, P. *et al.* The CO and N_2 abundance in comet P/Halley. *Astron. Astrophys.* **187,** 481–484 (1987).
7. Huebner, W. F., Boice, D. C. & Sharp, C. M. Polyoxymethylene in comet Halley. *Astrophys. J.* **320,** L149–L152 (1987).
8. Huntress, W. T., Allen, M. & Delitsky, M. Carbon suboxide in comet Halley? *Nature* **352,** 316–318 (1991).
9. Meier, R., Eberhardt, P., Krankowsky, D. & Hodges, R. R. The extended formaldehyde source in comet P/Halley. *Astron. Astrophys.* **277,** 677–690 (1993).
10. Greenberg, J. M. & Li, A. From interstellar dust to comets: the extended CO source in comet Halley. *Astron. Astrophys.* **332,** 374–384 (1998).
11. Chiar, J. E. *et al.* Processing of icy mantles in protostellar envelopes. *Astrophys. J.* **498,** 716–727 (1998).
12. Biver, N. *et al.* Substantial outgassing of CO from comet Hale–Bopp at large heliocentric distance. *Nature* **380,** 137–139 (1996).
13. Biver, N. *et al.* Evolution of the outgassing of comet Hale–Bopp (C/1995 O1) from radio observations. *Science* **275,** 1915–1918 (1997).
14. Womack, M., Festou, M. C. & Stern, S. A. The heliocentric evolution of key species in the distantly-active comet C/1995 O1 (Hale–Bopp). *Astron. J.* **114,** 2789–2795 (1997).
15. Greene, T. P., Tokunaga, A. T., Toomey, D. W. & Carr, J. S. CSHELL: A high spectral resolution 1–5 μm cryogenic echelle spectrograph for the IRTF. *Proc. SPIE* **1946,** 311–324 (1993).
16. Dello Russo, N., DiSanti, M. A., Mumma, M. J., Magee-Sauer, K. & Rettig, T. W. Carbonyl sulfide in comets C/1996 B2 (Hyakutake) and C/1995 O1 (Hale–Bopp): Evidence for an extended source in Hale–Bopp. *Icarus* **135,** 377–388 (1998).
17. Dello Russo, N. *et al.* Direct detection of water in comet C/1995 O1 (Hale–Bopp). *Icarus* (submitted).
18. Herzberg, G. *Spectra of Diatomic Molecules* (Van Nostrand Reinhold, New York, 1950).
19. Weaver, H. A. *et al.* Infrared spectroscopy of comet Hale–Bopp. *Earth Moon Planets* (in the press).
20. Lämmerzahl, P. *et al.* Expansion velocity and temperatures of gas and ions measured in the coma of comet P/Halley. *Astron. Astrophys.* **187,** 169–173 (1987).
21. Boice, D. C., Sablik, M. J. & Konno, I. Distributed coma sources and the CH_4/CO ratio in Comet Halley. *Geophys. Res. Lett.* **17,** 1813–1816 (1990).
22. Crifo, J. F. A general physicochemical model of the inner coma of active comets. 1. Implications of spatially distributed gas and dust production. *Astrophys. J.* **445,** 470–488 (1995).
23. Xie, X. & Mumma, M. J. Monte Carlo simulation of cometary Atmospheres: Application to Comet P/Halley at the time of the Giotto Spacecraft encounter. II. Axisymmetric model. *Astrophys. J.* **464,** 457–475 (1996).
24. Combi, M. R. Time-dependent gas kinetics in tenuous planetary atmospheres: The cometary coma. *Icarus* **123,** 207–226 (1996).
25. Xie, X. & Mumma, M. J. The effect of electron collisions on rotational populations of cometary water. *Astrophys. J.* **386,** 720–728 (1992).
26. Biver, N. *et al.* Long term evolution of the outgassing of comet Hale–Bopp from radio observations. *Earth Moon Planets* (in the press).
27. Kunde, V. G. & Maguire, W. C. A direct integration transmittance model. *J. Quant. Spectrosc. Rad. Transf.* **14,** 803–817 (1974).
28. Rothman, L. S. *et al.* The HITRAN molecular database: Editions of 1991 and 1992. *J. Quant. Spectrosc. Rad. Transf.* **48,** 469–507 (1992).
29. Crovisier, J. Rotational and vibrational synthetic spectra of linear parent molecules in comets. *Astron. Astrophys. Suppl.* **68,** 223–258 (1987).
30. Huebner, W. F., Keady, J. J. & Lyon, S. P. Solar photo rates for planetary atmospheres and atmospheric pollutants. *Astrophys. Space Sci.* **195,** 1–294 (1992).
31. Green, S. F., McDonnell, J. A. M., Pankiewicz, G. S. A. & Zarnecki, J. C. in *20th ESLAB Symposium on the Exploration of Halley's Comet* Vol. 2, 81–86 (SP-250, ESA, 1986).
32. Jewitt, D. & Matthews, H. E. Particulate mass loss from comet Hale–Bopp. *Astron. J.* **117,** 1056–1062 (1999).

Acknowledgements. This work was supported through the NASA Planetary Astronomy Program. We thank the staff of the NASA Infrared Telescope Facility for their support throughout our comet Hale–Bopp observing campaign. The IRTF is operated by the University of Hawaii under contract to NASA. We thank J. Crovisier for comments which improved the manuscript.

Correspondence and requests for materials should be addressed to M.D. (e-mail: disanti@kuiper.gsfc.nasa.gov).

Collective and plastic vortex motion in superconductors at high flux densities

A. M. Troyanovski*†, J. Aarts* & P. H. Kes*

** Kamerlingh Onnes Laboratory, Leiden University, PO Box 9504, 2300 RA Leiden, The Netherlands*
† Institute for High Pressure Physics, Russian Academy of Science, Troitsk, 142092, Russia

The 'mixed state' of type II superconductors occurs when magnetic flux penetrates the material (in the form of vortices) without destroying the superconducting ground state. Zero resistivity is retained if the vortices are pinned by crystalline defects, but is destroyed by vortex motion. This provides the practical motivation for studying vortices in random pinning potentials[1–7]. But the insights so obtained also bear on the more general class of problems involving the dynamics of elastic media in the presence

© 1999 Macmillan Magazines Ltd